Quantum Criticality in an Organic Magnet

M. B. Stone,[1,2] C. Broholm,[2,3] D. H. Reich,[2] O. Tchernyshyov,[2] P. Vorderwisch,[4] and N. Harrison[5]

[1]*Condensed Matter Sciences Division, Oak Ridge National Laboratory, Oak Ridge, Tennennesse 37831, USA*
[2]*Department of Physics and Astronomy, Johns Hopkins University, Baltimore, Maryland 21218, USA*
[3]*National Institute of Standards and Technology, Gaithersburg, Maryland 20899, USA*
[4]*Hahn-Meitner Institut, D-14109 Berlin, Germany*
[5]*National High Magnetic Field Laboratory, Los Alamos National Laboratory, Los Alamos, New Mexico 87545, USA*

(Received 17 March 2005; revised manuscript received 14 February 2006; published 29 June 2006)

Exchange interactions between $S = \frac{1}{2}$ sites in piperazinium hexachlorodicuprate produce a frustrated bilayer magnet with a singlet ground state. We have determined the field-temperature phase diagram by high field magnetization and neutron scattering experiments. There are two quantum critical points: $H_{c1} = 7.5$ T separates a quantum paramagnet phase from a three dimensional, antiferromagnetically ordered state while $H_{c2} = 37$ T marks the onset of a fully polarized state. The ordered phase, which we describe as a magnon Bose-Einstein condensate (BEC), is embedded in a quantum critical regime with short range correlations. A low temperature anomaly in the BEC phase boundary indicates that additional low energy features of the material become important near H_{c1}.

DOI: 10.1103/PhysRevLett.96.257203 PACS numbers: 75.10.Jm, 75.40.Gb, 75.50.Ee

The concept of a critical transition between different phases of matter at temperature $T = 0$ is central to many complex phenomena in strongly correlated systems [1]. Quantum critical points (QCPs) give rise to anomalous properties through a range of temperatures, and may be responsible for heavy fermions [2], non-Fermi liquids [3], and the anomalous normal state of doped cuprates [4]. Among the nonthermal tuning parameters accessible to the experimentalist, doping has been applied to access QCPs in heavy fermion intermetallics [5,6] and copper oxide superconductors [7], and hydrostatic pressure has been used to expose anomalous superconducting [8] and metallic [9] phases in weak itinerant magnets. While magnetic fields generally induce conventional transitions between states with static spin order, exceptions are found in anisotropic spin systems where a transverse magnetic field, H, can drive a transition from spin order at $H = 0$ to a quantum disordered state [10]. The reverse transition from a quantum paramagnet (QP) in zero field to an anisotropic ordered state in high fields has been observed in certain organo-metallics [11–13]. While materials with such behavior are often quasi-one-dimensional, recent experiments have revealed a wider range of cooperative phenomena in higher dimensional systems [14–16]. Owing to the simplicity of the low energy Hamiltonian, high field experiments on organo-metallic magnets are a promising route to new information about quantum criticality.

We provide a comprehensive analysis of the $H - T$ phase diagram of a quasi-two-dimensional (2D) frustrated organo-metallic antiferromagnet (AFM) with two field driven QCPs. Key results include a detailed characterization of a Bose-Einstein condensation (BEC) in the vicinity of a zero-temperature quantum critical point. We also find a low T anomaly in the BEC phase boundary, which may indicate that nuclear spins and/or phonons are important thermodynamic degrees of freedom close to the QCP.

Experiments were carried out on the quasi-2D $S = \frac{1}{2}$ quantum AFM piperazinium hexachlorodicuprate $[(C_4H_{12}N_2)Cu_2Cl_6 \equiv \text{PHCC}]$. The crystal structure is composed of Cu-Cl sheets in the **a**-**c** plane, separated by piperazinium layers [17,18]. Magnetic properties are dominated by the Cu-Cu interactions within individual sheets shown in Fig. 1. The magnetic connectivity is that of an oblique bilayer, with the strongest bond, i.e., the

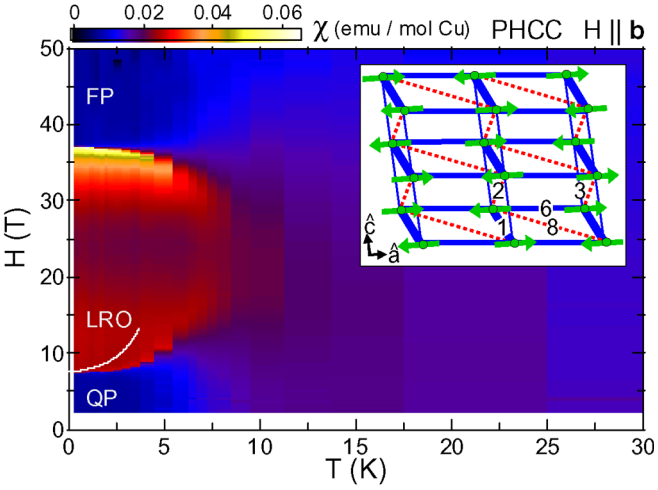

FIG. 1 (color online). Differential susceptibility $\chi(H, T)$ for PHCC. Solid white line for $H < 14.2$ T is the line of phase transitions defined by the onset of Néel order at higher field. The terms QP, LRO, and FP are explained in the text. Inset: PHCC structure showing the Cu^{2+} $S = \frac{1}{2}$ sites (solid circles) viewed along the **b** axis. Interacting spins are connected by lines with thickness proportional to the contribution to the $H = 0$ ground state energy. The red dashed [blue solid] bonds are frustrated [unfrustrated] and increase [decrease] the ground state energy. Numbering corresponds to Ref. [17]. Vectors show the ordered spin structure at $T = 1.65$ K and $H = 13.7$ T.

dimer, bond 1, providing interlayer coupling. Frustrated interlayer bonds 2 and 8 may also play a role in producing a singlet ground state with strong correlations to five near neighbors. Magnetic excitations at $H = 0$ are dominated by a dispersive triplet of magnons, also known as the triplon, with a bandwidth $W = 1.8$ meV and an energy gap $\Delta = 1$ meV. Cluster expansion analysis of the $H = 0$ dispersion indicates that the strongest intralayer bond $J_6 \approx 0.36J_1$, while the frustrating bonds J_2, J_8 are $\approx 0.1J_1$ [19]. An experimental limit of 0.2(1) meV has been placed on the out of plane dispersion and the triplons are degenerate to within 0.05 meV.

Magnetic susceptibility measurements were performed at the National High Magnetic Field Laboratory using a compensated-coil susceptometer in pulsed fields up to $H = 50$ T for $0.46\ \text{K} \leq T \leq 30$ K [20]. The sample was a 1.36 mg hydrogenous single crystal with $\mathbf{H} \parallel \mathbf{b}$. Elastic neutron scattering measurements were performed on the FLEX spectrometer at the Hahn-Meitner Institut (HMI). The sample was composed of two 89% deuterated single crystals with total mass 1.75 grams, coaligned within 0.5° and oriented in the $(h0l)$ scattering plane, $\mathbf{H} \parallel \mathbf{b}$. A room temperature graphite filter or a liquid nitrogen cooled beryllium filter was employed in the scattered beam for neutron energies 14.7 and 2.5 meV, respectively. Beam divergence was defined by the ^{58}Ni neutron guide before the monochromator and 60′ collimators elsewhere.

Differential magnetic susceptibility data, $\chi(H, T) = dM/dH$, are shown in Fig. 1. At $T = 0.46$ K there is evidence for two quantum transitions from gapped phases with $\chi = 0$ for $H < H_{c1} \approx 7.5$ T and $H > H_{c2} \approx 37$ T to a magnetizable state in the intermediate field range. $\chi(H)$ at the lower transition is shown in Fig. 2(a). Integrating $\chi(H, T = 0.46\ \text{K})$ yields a saturation magnetization of $1.10(5)\mu_B$ per spin, identifying the high field phase as fully spin-polarized (FP).

In the intermediate field phase AFM Bragg peaks were found at wave vectors $\mathbf{Q} = \tau + (0.5, 0, 0.5)$ where τ is a reciprocal lattice vector of the chemical cell. The lower bound on the order parameter correlation length in the **a**-**c** plane is $2.0(2) \times 10^3$ Å. Analysis of peak intensities yields the spin structure in Fig. 1, which is consistent with bond energies measured in the zero field phase in that (un)frustrated bonds correspond to (anti)parallel spins. Normalizing to incoherent scattering and assuming long-range order (LRO) along **b** yields $g\mu_B\langle S\rangle = 0.33(3)g\mu_B$ at $T = 1.65$ K and $H = 13.7$ T.

Figure 2 shows the order parameter onset in H and T sweeps. While the onset of Bragg scattering coincides with the onset of elevated $\chi(H)$ for $T \approx 0.4$ K, Bragg peaks first appear well within the high susceptibility state for $T \approx 3$ K. A similar conclusion is reached based on the T sweep at $H = 14.2$ T where the critical temperature for LRO is $T_c(14.2\text{T}) = 3.705(3)$ K compared to the $T \approx 8$ K onset of the high susceptibility state. The solid line for $H < 14.2$ T in Fig. 1 is the phase boundary inferred from neutron diffraction with further details in Fig. 3(a). For $T > 0.5$ K, the LRO phase resides well within the high susceptibility state.

At low T, the phase boundary to Néel order approaches the onset of the high susceptibility state, and for $T < 0.4$ K there is no intermediate phase that can be distinguished from the data. At lower T, field sweeps of the magnetic Bragg intensity, shown in Fig. 4(a), indicate a minimum in the phase boundary for $T \approx 0.2$ K. Plotted versus T in Fig. 4(b), these data show an intensity maximum for $T \approx 0.2$ K and $7.4 < H < 7.9$ T indicating that PHCC passes into and then back out of the LRO phase in this field range.

Figures 2 and 4 show a rounded onset of magnetic scattering in PHCC. If critical fluctuations are responsible for this, the energy scale must be less than the ≈ 50 μeV energy resolution. Alternatively, field inhomogeneity can

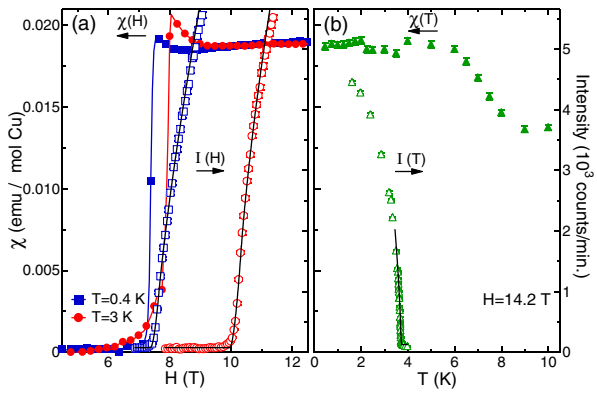

FIG. 2 (color online). (a) Field-dependence of $\chi(H)$ (filled symbols) at $T = 0.46$ K and 3 K, and of the $(\frac{1}{2}0\bar{\frac{1}{2}})$ AFM Bragg intensity $I(H)$ (open symbols) at $T = 0.42$ K and 2.85 K. The onset of 3D ordering occurs above H_{c1}. (b) Temperature dependence of $(\frac{1}{2}0\bar{\frac{1}{2}})$ Bragg peak at $H = 14.2$ T, compared to $\chi(H, T)$. Solid lines through $I(H)$ and $I(T)$ are fits as described in the text.

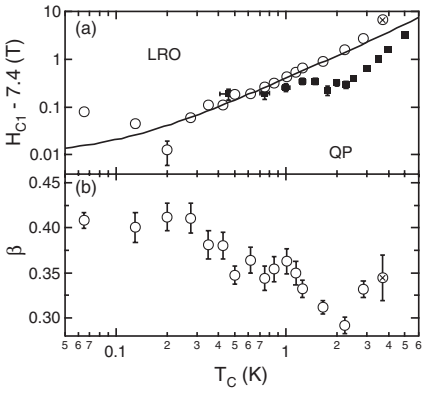

FIG. 3. (a) Phase diagram for PHCC near H_{c1}. Solid squares: onset of high susceptibility state. Open circles: onset of AFM LRO from fits described in the text. Absolute fields reported for open and closed symbols differ by less than 0.05 T. The solid line is the calculated mean-field BEC phase boundary. (b) Critical exponent for onset of LRO. Crossed symbols are from the T-dependent data, $I(T)$, in Fig. 2(b).

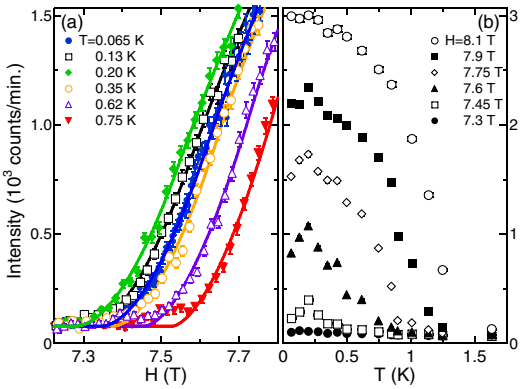

FIG. 4 (color online). Magnetic field (a) and temperature (b) dependent scattering intensity of the $(\frac{1}{2}0\bar{\frac{1}{2}})$ AFM Bragg peak, showing reentrant behavior of the gapped phase near H_{c1}. Solid lines are fits to model described in text. The temperature dependence was extracted from multiple field sweeps through binning with $\Delta H = 0.1$ T.

smear a singular onset. The solid lines in Figs. 2 and 4(a) were obtained by fitting $I(H) \propto (H - H_c)^{2\beta}$ and $I(T) \propto (T_c - T)^{2\beta}$ including the width of a rectangular field distribution as a fitting parameter along with H_c, T_c, and the critical exponent, β. While a 3.6(1)% distribution width accounts for the data, it exceeds the $\approx 1\%$ width expected for the HMI magnet. An additional potential source of static broadening are impurities that produce effective random fields [21].

Systematic values for $H_c(T)$ and β were obtained by fitting the following expression $\Delta I(H, T) \propto M(H, T)^2 \propto [H - H_c(T)]^{2\beta}$ to data in Figs. 2 and 4(a) restricted to the ranges $H < H_c + 0.75$ T and $T > T_c - 0.33$ K. The apparent distribution width for the applied field, H, was fixed at 3.6%. The corresponding phase boundary in Fig. 3(a) affirms the existence of a wedge in $H - T$ space with neither LRO nor a spectral gap. Taylor expansion of the phase boundary about a generic point (H_c, T_c) on the line of transitions, $H_c(T) \approx H_c(T_c) + H_c'(T_c)(T - T_c)$, shows that if $M(H, T) \propto [H - H_c(T)]^{\beta}$ then $M(H_c, T) \propto [H_c'(T_c)(T_c - T)]^{\beta}$. Hence the consistent values of β extracted from H and T scans at $T \approx 3.5$ K instill confidence in the experiment and analysis [see Fig. 3(b)].

It is well-known that the field-induced phase transition to long-range order for antiferromagnets with an axial symmetry can be described as a BEC of magnons [22–24]. An applied field drives the chemical potential for spin-polarized magnons ($S_z = 1$) to zero causing BEC at sufficiently low T. In 2D, BEC can only occur at $T = 0$ so we associate the sharp increase in $\chi(H)$ indicated by solid points in Figs. 2(a) and 3(a) with the corresponding finite temperature quantum critical regime. In the immediate vicinity of the LRO phase boundary the critical phase is denoted renormalized classical (RC) [25] though there are no notable distinctions between the RC and QC regimes in the present data. The RC regime is characterized by a small population of magnons that behave as individual particles.

The finite T transition to Néel order may be BEC resulting from weak inter-bilayer coupling or a 2D Kosterlitz-Thouless (KT) transition. To distinguish these scenarios we explore the corresponding theoretical phase boundaries. Following Nikuni *et al.* [24] and Misguich and Oshikawa [26] we treat magnons as bosons with a chemical potential $\mu = g\mu_B[H - H_c(0)]$ and short range repulsion, v_0:

$$\mathcal{H} = \sum_{\mathbf{k}} (\epsilon_{\mathbf{k}} - \mu) a_{\mathbf{k}}^{\dagger} a_{\mathbf{k}} + \frac{v_0}{V} \sum_{\mathbf{q},\mathbf{k},\mathbf{k}'} a_{\mathbf{q}+\mathbf{k}'}^{\dagger} a_{\mathbf{q}-\mathbf{k}'}^{\dagger} a_{\mathbf{q}-\mathbf{k}} a_{\mathbf{q}+\mathbf{k}}. \tag{1}$$

Mean-field theory yields a condensate magnon density $n = M/M_{\mathrm{sat}} = g\mu_B[H - H_c(0)]/2v_0$. Beyond a cusp that may be associated with logarithmic corrections [27], Fig. 2(a) shows that the low T $\chi(H)$ indeed displays a plateau from which we obtain $v_0/V = 1.9$ meV, where V is the unit cell volume. As expected for hard core bosons, this number is similar to the magnon bandwidth $W = 1.8$ meV.

The Hartree Fock approximation provides the effective Hamiltonian

$$\mathcal{H} = \sum_{\mathbf{k}} (\epsilon_{\mathbf{k}} - \mu + v_0 n) a_{\mathbf{k}}^{\dagger} a_{\mathbf{k}}. \tag{2}$$

Bosons condense when the renormalized chemical potential $\tilde{\mu} \equiv \mu - 2v_0 n_c = 0$, which yields the critical density and field

$$n_c(T) = \frac{1}{V} \sum_{\mathbf{k}} \frac{1}{\exp(\epsilon_{\mathbf{k}}/T) - 1}, \tag{3}$$

$$H_c(T) = H_c(0) + 2v_0 n_c(T)/g\mu_B. \tag{4}$$

We assume quasi-2D magnon dispersion $\epsilon_{\mathbf{k}} = \epsilon_{\mathbf{k}}^{2D} + 2\gamma[1 - \cos(k_y b)]$ with $\epsilon_{\mathbf{k}}^{2D}$ from experiments [17]. When $T \ll \gamma$, only the bottom of the magnon band is thermally excited and one may replace the exact band structure with parabolic dispersion to obtain

$$n_c(T) = \zeta(3/2)\left(\frac{m^{3\mathrm{D}} T}{2\pi\hbar^2}\right)^{3/2}, \tag{5}$$

where $m^{3\mathrm{D}} = (m_a m_b m_c)^{1/3}$ is the 3D effective mass. In the limit of a very weak inter-bilayer tunnelling there is a regime $\gamma \ll T \ll W$ where the in-plane dispersion can be treated as parabolic and the critical density for a quasi-2D Bose gas is obtained [28]

$$n_c(T) = \frac{m^{2\mathrm{D}} T}{2\pi\hbar^2 b} \log\frac{2T}{\gamma}. \tag{6}$$

Here $m^{2\mathrm{D}} = (m_a m_c)^{1/2}$ and b is the inter-bilayer distance. In the intermediate regime $T = \mathcal{O}(\gamma)$ the critical density first rises *faster* than $T^{3/2}$ [26] before crossing over to $T \log T$ behavior. For $\gamma = 0.03$ meV the calculated phase boundary shown in Fig. 3(a) is consistent with the data over one decade of T. If bilayers in PHCC were fully decoupled from each other the BEC would change into a KT vortex-unbinding transition. In 2D the crossover exponent $\phi = 1$, so in contrast to the observed phase boundary a KT phase

boundary $H_c(T) = H_c(0) + CT^{\phi}$ would be linear for $T \rightarrow 0$. This is consistent with a recent comprehensive analysis of magnon condensation in 2D by Sachdev and Dunkel [29]. Hence it appears that 3D BEC rather than vortex unbinding is the appropriate description of the field-induced transition to LRO in PHCC.

The experimental high T limit for the critical exponent $\beta = 0.34(2)$ obtained by averaging PHCC data for $0.5\ \mathrm{K} < T < 4\ \mathrm{K}$ is consistent with a 3D XY model for which $\beta = 0.345$ [30]. Upon cooling through the temperature $T \approx 0.4$ K where $H_c(T)$ merges with the 2D BEC crossover inferred from magnetization data, the experimental values for β increase. The apparent increase of the exponent β is consistent with an expected crossover from a thermally driven transition to a quantum phase transition. Because the upper critical dimension of the zero-temperature BEC is $d_c = 2$ [31], β has a mean-field value of $\frac{1}{2}$.

A discrepancy in the description of the phase diagram for PHCC presented so far exists for $T < 0.3$ K where the observed critical field exceeds the BEC phase boundary [Eqs. (4) and (3)] with a finite $T \approx 0.2$ K minimum (Figs. 3 and 4). Various low energy aspects of PHCC may be responsible for this behavior. For example, measurements of the dependence of H_{c1} on field orientation [32] indicates g-factor anisotropy in the range $2.1 < g^{\alpha\alpha} < 2.35$. This provides an estimate for exchange anisotropy of ≈ 0.1 meV [33], which could lead to an Ising transition at sufficiently low T. Alternatively nuclear spins and phonons which are effectively decoupled from magnetism at high T and normally unimportant compared to exchange interactions at low T may become relevant close to the field tuned QCP. Similar low T anomalies have been found in other electronic spin systems close to quantum criticality such as GGG [34], $LiHoF_4$ [10], and $ZnCr_2O_4$ [35]. In $LiHoF_4$, the anomaly favors the spin ordered phase and is associated with hyperfine coupling to the nuclear spin system. The spin ordered phase is also favored for $ZnCr_2O_4$ where the anomaly is associated with magneto-elastic coupling. Low temperature spin-lattice coupling is also observed in the spin-gap systems $TlCuCl_3$ [36] and CuHpCl [37]. For PHCC, the singlet ground state may be affected by coupling to Cu nuclear spins for $T < 0.2$ K. This could help to stabilize bond order over spin order and explain our failure to discover additional phase boundaries at low T. Alternatively, $H = 7.4$ T and $T = 0.2$ K may be a tetra-critical point separating the bond ordered phase, the (0.5, 0, 0.5) type spin ordered phase and a yet to be detected magneto-elastic or nuclear + electronic spin ordered phase.

The $H - T$ phase diagram for PHCC illustrates many important aspects of strongly correlated systems. There is evidence for a finite T crossover to a quasi-2D RC phase with 3D BEC at lower T and higher H. We also presented evidence for a nonmonotonic phase boundary to spin order at low T, which indicates that exchange anisotropy, nuclear spin, and/or lattice degrees of freedom can be important close to quantum criticality.

We gratefully acknowledge discussions with A. Aharony, L. Balents, O. Entin-Wohlmann, A. B. Harris, S. Sachdev, and T. Yildirim. Work at JHU was supported by the NSF through Grants No. DMR-0074571, No. DMR-0306940, and No. DMR-0348679 and by the BSF through Grant No. 2000-073. ORNL is managed for the US DOE by UT-Battelle Inc. under Contract No. DE-AC05-00OR2272.

[1] S. Sachdev, *Quantum Phase Transitions* (Cambridge University Press, Cambridge, England, 2001).
[2] G. Aeppli and C. Broholm, in *Handbook on the Physics and Chemistry of Rare Earths* (Elsevier, New York, 1994), Vol. 19, Ch. 131, p. 123.
[3] P. Coleman and C. Pépin, Physica (Amsterdam) **312B**, 383 (2002).
[4] C. M. Varma, Phys. Rev. Lett. **83**, 3538 (1999).
[5] A. Schroeder *et al.*, Int. J. Mod. Phys. B **16**, 3031 (2002).
[6] S. Mederle *et al.*, J. Phys. Condens. Matter **14**, 10 731 (2002).
[7] J. M. Tranquada *et al.*, Phys. Rev. B **54**, 7489 (1996).
[8] S. S. Saxena *et al.*, Nature (London) **406**, 587 (2000).
[9] F. M. Grosche *et al.*, J. Phys. Condens. Matter **12**, L533 (2000).
[10] D. Bitko *et al.*, Phys. Rev. Lett. **77**, 940 (1996).
[11] J. Eckert *et al.*, Phys. Rev. B **20**, 4596 (1979).
[12] G. Chaboussant *et al.*, Eur. Phys. J. B **6**, 167 (1998).
[13] Z. Honda *et al.*, Phys. Rev. Lett. **81**, 2566 (1998).
[14] N. Cavadini *et al.*, Int. J. Mod. Phys. B **16**, 3302 (2002).
[15] M. B. Stone *et al.*, Phys. Rev. B **65**, 064423 (2002).
[16] M. Jaime *et al.*, Phys. Rev. Lett. **93**, 087203 (2004).
[17] M. B. Stone *et al.*, Phys. Rev. B **64**, 144405 (2001).
[18] L. P. Battaglia *et al.*, J. Chem. Soc. Dalton Trans. **2**, 265 (1988).
[19] H.-J. Mikeska and M. Müller, Appl. Phys. A **74**, S580 (2002).
[20] We supress μ_o in units of magnetic field for convenience.
[21] S. Fishman and A. Aharony, J. Phys. C **12**, L729 (1979).
[22] T. Matsubara and H. Matsuda, Prog. Theor. Phys. **16**, 569 (1956).
[23] I. Affleck, Phys. Rev. B **41**, 6697 (1990).
[24] T. Nikuni, M. Oshikawa, A. Oosawa, and H. Tanaka, Phys. Rev. Lett. **84**, 5868 (2000).
[25] S. Chakravarty *et al.*, Phys. Rev. B **39**, 2344 (1989).
[26] G. Misguich and M. Oshikawa, J. Phys. Soc. Jpn. **73**, 3429 (2004).
[27] S. Sachdev *et al.*, Phys. Rev. B **50**, 258 (1994).
[28] R. Micnas, J. Ranninger, and S. Robaszkiewicz, Rev. Mod. Phys. **62**, 113 (1990).
[29] S. Sachdev and E. R. Dunkel, Phys. Rev. B **73**, 085116 (2006).
[30] M. F. Collins, *Magnetic Critical Scattering* (Oxford University Press, New York, 1989).
[31] M. P. A. Fisher *et al.*, Phys. Rev. B **40**, 546 (1989).
[32] M. B. Stone *et al.* (unpublished).
[33] T. Moriya, Phys. Rev. **120**, 91 (1960).
[34] Y. K. Tsui *et al.*, Phys. Rev. Lett. **82**, 3532 (1999).
[35] S. H. Lee *et al.*, Phys. Rev. Lett. **84**, 3718 (2000).
[36] O. Vyaselev *et al.*, Phys. Rev. Lett. **92**, 207202 (2004).
[37] J. E. Lorenzo *et al.*, Phys. Rev. B **69**, 220409(R) (2004).